Cite this article
Mrak M, Daneu N and Dolenec S
Hydration of belite–ye'elimite–ferrite cement with addition of red mud and waste concrete.
Advances in Cement Research,
https://doi.org/10.1680/jadcr.25.00024

Research Article
Paper 2500024
Received 27/01/2025; Accepted 03/10/2025

Advances in Cement Research

Hydration of belite–ye'elimite–ferrite cement with addition of red mud and waste concrete

Maruša Mrak
Slovenian National Building and Civil Engineering Institute, Ljubljana, Slovenia (Orcid:0000-0002-8978-7916)

Nina Daneu
Jožef Stefan Institute, Ljubljana, Slovenia (Orcid:0000-0003-2740-1448)

Sabina Dolenec
Slovenian National Building and Civil Engineering Institute, Ljubljana, Slovenia; Department of Geology, Natural Sciences and Engineering, University of Ljubljana, Ljubljana, Slovenia (Orcid:0000-0003-0483-9623) (corresponding author: sabina.dolenec@zag.si)

The hydration kinetics, phase assemblage, microstructure and mechanical properties of belite–ye'elimite–ferrite (BYF) cement containing different secondary raw materials (red mud and waste concrete) and cured at 5, 20 or 60°C were examined. Different secondary raw materials were found to lead to changes in cement hydration. The influence of these materials on the hydration processes of belite and ferrite became more noticeable at a curing temperature of 5°C, but diminished with an increase in curing temperature. The BYF cement made with red mud exhibited accelerated hydration, particularly at 5°C, due to higher contents of mayenite and alkali sulfate compared with cement with natural materials and waste concrete. Red mud inhibited early ettringite formation due to the presence of aphthitalite but promoted monosulfate through accelerated ye'elimite hydration. Ferrite hydration was delayed by red mud, as alkali sulfates promote belite reactivity and calcium silicate hydrate (C-S-H) formation over strätlingite. Periclase increased siliceous hydrogarnet formation at higher temperatures, supporting delayed yet stable strength development. The curing temperature impacted the morphology of the C-S-H (transitioning from a fine fibrillar-like structure to a foil-like structure) and affected the chemical composition of hydrates, resulting in a lower incorporation of iron in hydrogarnet and C-S-H at higher temperatures. Increased curing temperatures promoted aluminium uptake in calcium aluminium silicate hydrate.

Keywords: belite–ye'elimite–ferrite (BYF) cement/cement/cement paste/cementitious materials/hydrated cement/secondary raw materials/temperature

Introduction

Currently, the general direction in the cement industry is to employ alternative raw materials in the manufacture of cement clinker. With this in mind, various materials, particularly waste and by-products generated from different industrial processes, have been suggested as potential substitutes (Galbenis and Tsimas, 2006).

In recent years, researchers have shown significant interest in construction and demolition waste (CDW), which is generated in large quantities worldwide (Gastaldi *et al*., 2015). The construction sector alone produces over 3 billion tonnes of CDW annually, representing a significant material source for cement production (Akhtar and Sarmah, 2018). The predominant use of concrete from CDW is as recycled aggregates in the production of mortar and concrete. However, these aggregates are of lower quality due to residual hydrated cement, which negatively affects the concrete's properties and strength (Gastaldi *et al*., 2015), (Kou *et al*., 2011). The fine fraction of concrete waste, comprising residual cement and aggregates, is also used as a clinker substitute, permissible under cement standards such as EN 197-6 (Oliveira *et al*., 2020). The recycling of these materials into cement production provides a sustainable solution by reducing landfill waste and provides an alternative to natural aggregates or clinker substitutes.

Another industrial residue is red mud, which is derived from the Bayer alumina production process using bauxite ore (Zhang *et al*., 2011). With an annual global production of approximately 70 Mt, its highly alkaline nature poses environmental risks, including soil and groundwater contamination. (Vangelatos *et al*., 2009). Recycling red mud in cement production offers an eco-friendly solution by reducing landfill waste and utilising it as a clinker substitute (Jun *et al*., 2019; Manfroi *et al*., 2014; Zhang *et al*., 2011).

Belite–ye'elimite–ferrite (BYF) cements provide an opportunity to integrate industrial residues into clinker production, reducing their environmental footprints (Álvarez-Pinazo *et al*., 2016; Gartner, 2017; Telesca *et al*., 2019). However, the incorporation of such materials introduces minor elements (e.g. iron, alkalis, phosphorus and heavy metals) into the clinker (Bullerjahn *et al*., 2015). These elements can form secondary phases such as mayenite, gehlenite, periclase and various alkali sulfates, which influence the hydration kinetics, pore structure and early-age properties of the cement paste (Baltakys *et al*., 2021; Bullerjahn *et al*., 2015). In addition, the effect of these minor phases varies significantly at different curing temperatures.

Mayenite ($C_{12}A_7$) has gained attention for its ability to accelerate cement hydration due to its rapid dissolution, which alters the

calcium/aluminium ratio, promoting ettringite formation and sulfate depletion (Bullerjahn *et al*., 2019a; He and Li, 2018). Research indicates that mayenite accelerates hydration at low temperatures, typical of slow reactions, while the effect is less pronounced or slightly delayed at high temperatures (Koehler *et al*., 2022). These changes influence the microstructure and compressive strength of hydrated products (Bullerjahn *et al*., 2019a, 2019b). Numerous investigations by various authors have focused on the hydration of pure mayenite (Edmonds and Majumdar, 1988; Koplík *et al*., 2014) and the results have shown that higher temperatures enhance phase reactivity and reduce their initial hydration period. Gehlenite (C_2AS), although considered weakly hydraulic, can react to form strätlingite over time (Dolenec *et al*., 2020; Winnefeld *et al*., 2017). Its reactivity increases with a finer particle size or as glass with gehlenite composition (Snellings, 2013). In calcium aluminate cements, gehlenite partially reacts at elevated temperatures due to its higher aluminium oxide content (Scrivener and Capmas, 1998). Periclase (MgO), often added to raw meal, enhances reactivity and clinker formation (Liu *et al*., 2017; Wang *et al*., 2011), thus enhancing performance and reducing the energy required for grinding (De Souza *et al*., 2008). Controlled amounts of periclase dissolve into clinker phases, while excess crystallises as periclase (Kurdowski, 2014). The presence of various alkali sulfates can be observed in cement clinker, including arcanite (K_2SO_4), thenardite (Na_2SO_4), aphthitalite ($K_3N\overline{S}_4$) and calcium langbeinite ($KC_2\overline{S}_3$) (Ma and Qian, 2018; Taylor, 1999). According to Kumar and Kameswara Rao (1994), the introduction of arcanite and thenardite leads to a delay in setting time. Alkali ions accelerate setting, while sulfate ions delay it (Samet and Sarkar, 1997). These compounds promote early strength development but may reduce long-term compressive strength (Sun *et al*., 2018; Taylor, 1997). Aphthitalite, in particular, slows early hydration but shortens the induction period, enhancing the acceleration phase (Huang *et al*., 2018).

Despite the significant research that has been conducted into the effects of various minor phases on cement hydration, particularly with respect to Portland cement, notable major gaps remain in understanding how these minor phases influence cement hydration at different temperatures, especially below or above ambient temperature. Knowledge regarding the effects of minor phases due to the introduction of different secondary raw materials in cement clinker on the hydration and strength of BYF cements remains quite limited, with no reported studies examining their effects across different temperatures. A previous study by the authors on the hydration of BYF cement with bottom ash (Mrak *et al*., 2024, 2021) highlighted the influence of calcium sulfate, clinker composition and temperature on hydration kinetics, hydrate assemblage and mechanical properties. However, the role of other minor phases was not considered. This study addresses this gap by investigating the effects of red mud and waste concrete, which were selected for their availability, adverse environmental affects and performance benefits. Incorporating these industrial residues into BYF cements offers the dual benefit of addressing waste management challenges while reducing the environmental footprint of cement production. This work bridges a critical gap in understanding the role of minor phases introduced by industrial residues in BYF cement hydration, particularly under varying temperatures, which has not been studied in detail previously. From a sustainability perspective, this research highlights the potential to repurpose hazardous and voluminous industrial residues into valuable construction materials, reducing environmental impact while supporting the circular economy concept.

In this study, the physico-mechanical properties and hydration evolution of BYF cement containing different secondary raw materials were investigated under curing temperatures of 5, 20 and 60°C. The composition of the hydration products was studied using X-ray powder diffraction (XRD) and thermogravimetric analysis (TGA). Compressive strength and porosity were determined and hydration kinetics was studied. Furthermore, selected samples were studied by nuclear magnetic resonance (NMR). The microstructure of hydrated samples and chemical composition of hydrates was assessed by transmission electron microscopy (TEM).

Materials and methods

Materials

BYF cement clinkers with a targeted phase composition of 65 wt% belite (C_2S), 20 wt% ye'elimite ($C_4A_3\overline{S}$) and 10 wt% ferrite (C_4AF) were synthesised. Three clinkers were prepared.

- CNAT was prepared using natural raw materials (limestone (Salonit Anhovo quarry), flysch (Salonit Anhovo quarry), bottom ash (Monfalcone power plant), white titanogypsum (Cinkarna Celje), calcined bauxite (Calucem) and mill scale (SIJ Acroni).
- CCON was prepared with waste concrete (provided by Salonit Anhovo cement plant).
- CRMD incorporated red mud from Hungary.

The chemical composition of the waste concrete and red mud was determined using X-ray fluorescence (XRF) analyses (see Table S1 in the online supplementary material (OSM)). The chemical compositions of natural raw materials are provided elsewhere (Borštnar *et al*., 2020). The materials were proportioned using the modified Bogue method (Chen and Juenger, 2011) (see Table S2 in the OSM).

The synthesis of the cement clinkers is detailed by Borštnar *et al*. (2020). XRF analyses of the clinkers were performed according to BS EN 196-2:2013 (BSI, 2013) (Table 1), while their mineralogical compositions were derived from XRD (Table 2). Used CDW contains a lot of magnesium oxide (MgO), leading to a high amount of periclase in the cement clinker. Red mud contains significant amounts of ferric oxide (Fe_2O_3), aluminium oxide (Al_2O_3) and other oxides, leading to the formation of greater amounts of minor phases such as mayenite and alkali sulfates.

Table 1. Results of chemical analysis of cement clinkers

	CNAT	CCON	CRMD
Calcium oxide (CaO): wt%	54.50	54.19	54.20
Silicon dioxide (SiO_2): wt%	22.60	22.36	22.33
Aluminium oxide (Al_2O_3): wt%	11.59	11.68	11.31
Ferric oxide (Fe_2O_3): wt%	3.34	3.53	3.80
Magnesium oxide (MgO): wt%	1.65	3.95	1.54
Potassium oxide (K_2O): wt%	0.77	0.73	0.72
Sodium oxide (Na_2O): wt%	0.31	0.30	0.47
Titanium dioxide (TiO_2): wt%	0.67	0.67	0.76
Phosphorus pentoxide (P_2O_5): wt%	0.07	0.07	0.07
Chromium(III) oxide (Cr_2O_3): wt%	0.07	0.07	0.08
Manganese oxide (MnO): wt%	0.07	0.09	0.07
Sulfur trioxide (SO_3): wt%	2.54	2.42	2.14
Loss on ignition: wt%	0.20	0.50	2.30
Total	98.38	100.56	99.79

Table 2. Phase compositions of the cement clinkers, determined by XRD and Rietveld refinement

	CNAT	CCON	CRMD
β-Dicalcium silicate (belite): wt%	65.7	63.5	64.4
γ-Dicalcium silicate: wt%	3.8	3.3	4.2
Ye'elimite orthorhombic: wt%	9.1	9.2	8.2
Ye'elimite cubic: wt%	7.0	7.7	6.2
Ferrite: wt%	7.4	8.5	9.3
Mayenite: wt%	3.4	2.5	3.8
Gehlenite: wt%	0.5	0.5	0.7
Periclase: wt%	1.2	3.3	1.1
Arcanite: wt%	1.0	0.9	0.5
Aphthitalite: wt%	0.9	0.6	1.6

Cement mixtures were prepared by blending ground clinkers with white titanogypsum in order to achieve a calcium sulfate to ye'elimite molar ratio of 1.5. The cements were further processed in a ball mill (Capco Test Equipment model 9VS). The Blaine fineness of each cement mixture was determined to be 4880 ± 20 cm^2/g. The particle size distributions of the cements were determined using a laser particle analyser (SYNC Microtrac MRB) (see Figure S1 in the OSM).

A water/cement ratio of 0.5 was used for the hydration experiments. The cement pastes were manually mixed for 3 min using a spatula, then cast into prismatic moulds (10 mm × 10 mm × 25 mm). After 24 h, the specimens were demoulded and cured in sealed plastic containers at a temperature of 5, 20 or 60°C. Hydration was stopped by solvent exchange using isopropanol and diethyl ether (Snellings *et al*., 2018) at 1, 7, 28, 90 and 180 days and the samples were analysed by XRD, TGA, NMR, TEM and mercury intrusion porosimetry (MIP).

Methods

Isothermal conduction calorimetry was conducted on samples cured at 5, 20 and 60°C using a TAM Air device (TA instruments). The procedure involved 3 min of manually mixing 4 g of the prepared cement with 2 g of deionised water. The mixture was transferred into a glass ampoule, capped and placed directly into the calorimeter for testing.

XRD analysis of the cement clinkers and pastes was performed using a PANalytical Empyrean X-ray diffractometer equipped with CuK_α radiation. The detector used was an X'Celerator, and the instrument was operated at a voltage of 45 kV and a current of 40 mA. To minimise the effects of the preferred orientation, the samples were back loaded into a circular sample holder with a diameter of 27 mm. The measurements were carried out in a 2θ range of 5–75° with a step size of $2\theta = 0.017°$. The data obtained were subjected to Rietveld refinement using PANalytical X'Pert High Score Plus diffraction software (version 4.9). The crystal structures proposed by Snellings (2016) were used, along with those provided by Cuesta *et al*. (2014, 2013) for the orthorhombic and cubic ye'elimite structures. For the quantification of amorphous content and poorly crystalline phases, the *G*-factor method (Jansen *et al*., 2011; O'Connor and Raven, 1988) was employed, with corundum (Al_2O_3, NIST SRM 676a) serving as the external standard. The results were normalised to 100 g of dry binder, incorporating the amount of bound water determined by TGA.

TGA of the cement pastes was conducted using a Netzsch STA 409 instrument, under a nitrogen atmosphere, using a heating rate of 10 K/min and covering a temperature range of 30–980°C. Alumina crucibles were used, with approximately 15 mg of sample. Chemically bound water was calculated from the weight loss up to 550°C and normalised to 100 g of dry binder (Lothenbach *et al*., 2016).

NMR spectra (^{29}Si magic angle spinning (MAS) and ^{27}Al MAS) were obtained for NAT (prepared using natural raw materials) samples at 90 days of hydration at different curing temperatures. Solid-state MAS NMR spectra were recorded on a Bruker Avance Neo 400 MHz NMR spectrometer equipped with a 4 mm CP-MAS probe. Larmor frequencies of ^{27}Al and ^{29}Si nuclei were 104.26 MHz and 79.48 MHz. Sample MAS frequencies were 15 kHz for the measurements. ^{27}Al spectra were recorded using a single pulse sequence of $\pi/2$ with a duration of 3.8 µs, 4096 scans and a delay between scans of 1 s. ^{29}Si spectra were recorded using a single pulse sequence of $\pi/2$ with a duration of 3.84 µs, 982 scans and a delay between scans of 60 s. The shift axis in all the spectra was referenced using an external reference of adamantane.

Freshly fractured surfaces of the NAT mixture with hydration stopped at 90 days at different temperatures were investigated by TEM to observe the morphology of the crystalline and amorphous phases and to determine their chemical composition. Samples were thinned by ion milling and then carbon-coated. The analyses were performed on a FEG-TEM JEM 2010 F (Jeol Ltd, Tokyo, Japan) with a 200 kV electron source and equipped with an energy-dispersive X-ray spectrometer (EDXS; Oxford

Instruments ISIS 300). Around 50 points were analysed per temperature.

Prepared cement pastes with a water/cement ratio of 0.5 were cast in 10 mm × 10 mm × 25 mm moulds and cured at either 5, 20 or 60°C at a relative humidity of 95 ± 2%. The samples were demoulded after 24 h. After 1, 7, 28, 90 and 180 days, the compressive strengths of the samples were determined using a ToniNorm, Toni Technic (by Zwick) testing machine. A loading rate of 0.05 kN/s was used, and measurements were conducted on three prisms for each curing age.

The porosity of the cement samples (NAT (natural raw materials), CON (concrete waste) and RMD (red mud), cured at different temperatures, was examined after 90 days of hydration using MIP. The porosity depending on the hydration time was examined on the NAT cement mixture at 20°C. After hydration stoppage, small representative pieces of each sample were analysed within the range of 0–414 MPa using penetrometers for solid substrates using a Micromeritics Autopore IV 9500 equipment (Micromeritics, Norcross, GA, USA). Two measurements were performed for each sample.

Results and discussion

Isothermal calorimetry results

The heat of hydration of NAT, CON and RMD at different curing temperatures is shown in Figure 1. The presence of mayenite significantly affected the kinetics, and also strongly depended on the curing temperature. At a curing temperature of 5°C, RMD (with the highest mayenite content) exhibited the fastest hydration and the shortest induction period, with a main peak at 18 h (Figure 1(a)). In contrast, CON (with the lowest mayenite content) reacted the slowest, showing its main peak at 24 h. This suggests that mayenite accelerates hydration, particularly at low temperatures (Bullerjahn *et al*., 2019a; He and Li, 2018; Koplík *et al*., 2014). At curing temperatures of 20°C and 60°C, the impact of mayenite was less pronounced (Koehler *et al*., 2022), although CON consistently reacted more slowly, with main peaks delayed compared with NAT and RMD. At 20°C, all the mixtures displayed a shoulder before the first peak, which was the smallest for RMD (Figure 1(b)). This corresponds to lower ettringite formation in RMD at 1 day, as indicated by the XRD analysis, as this peak is usually attributed to the hydration of ye'elimite and consequently the precipitation of ettringite. The maximum peak, which represents the precipitation of monosulfate (and/or ettringite) was greatest in RMD. At 60°C, two maximum peaks were observed (Figure 1(c)), with the second peak being higher, as more monosulfate forms than ettringite due to the higher solubility of ettringite at elevated temperatures (Lothenbach *et al*., 2008; Wang *et al*., 2017). Hydration kinetics are also influenced by alkali sulfates (arcanite, aphthitalite), which enhance the acceleration period (Ma and Qian, 2018; Sun *et al*., 2018) across all temperatures. Although the mayenite content was identified as a key contributor to hydration acceleration in RMD, other factors such as alkali sulfate content and overall clinker phase assemblage may also influence hydration behaviour.

The results therefore indicate that adding red mud accelerated the hydration process at low temperatures due to its higher mayenite content (Koehler *et al*., 2022) (due to the distinct chemical composition of red mud), which is beneficial for construction in cold environments. The addition of waste concrete slowed the hydration kinetics, which may be advantageous for applications requiring extended working times. At higher temperatures, RMD and CON exhibited smaller differences in hydration behaviour, with RMD maintaining slightly faster reactions. Red mud promotes greater monosulfate formation and reduces early ettringite precipitation (Lothenbach *et al*., 2008; Wang *et al*., 2017), potentially influencing the durability and strength evolution of cement.

The cumulative heat at 7 days was comparable across mixtures at all curing temperatures but slightly lower in CON at 5°C and 60°C, and in RMD at 20°C (Table 3). As the curing temperature

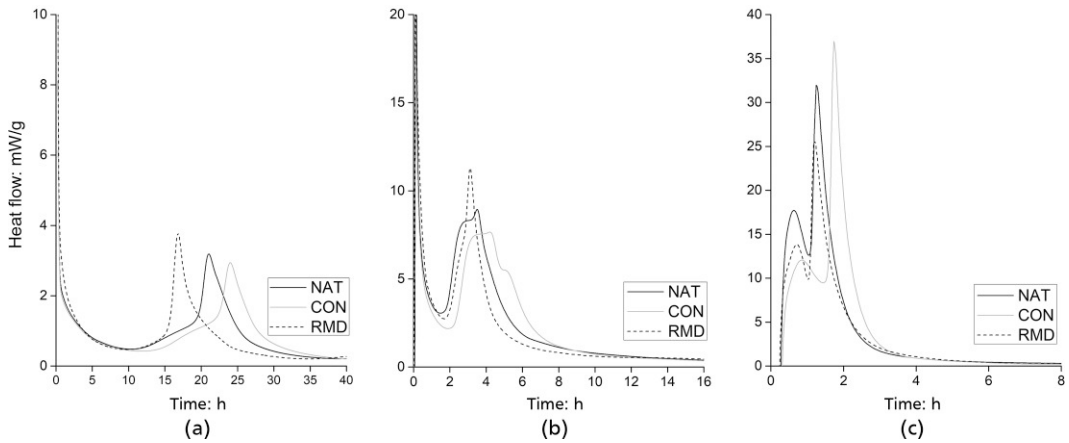

Figure 1. Hydration heat flows (normalised to the weight of cement) of NAT, CON and RMD cements after curing at: (a) 5°C; (b) 20°C; (c) 60°C

Table 3. Cumulative heat after 7 days of hydration, normalised to the weight of the cement, in the NAT, CON and RMD cements cured at 5, 20 and 60°C

	Cumulative heat: J/g		
Curing temperature: °C	NAT	CON	RMD
5	194	186	195
20	222	221	212
60	188	182	184

was increased from 5°C to 20°C, the cumulative heat in all the mixtures increased. However, at 60°C, it decreased, consistent with observations of Mrak *et al*. (2024). As reported elsewhere, after a long time, hydration decelerates more quickly at elevated temperatures (Chitvoranund, 2021) and lower degrees of hydration are often obtained (Lothenbach *et al*., 2007).

XRD and TGA results

The XRD patterns of the NAT at 5, 20 and 60°C are shown in Figure 2. The XRD patterns on CON and RMD are available in the OSM (Figures S2 and S3). The TGA results for 20°C curing are shown in Figure 3, while those at the other curing temperatures are shown in S4 and S5 of the OSM. Other phase quantifications at various hydration times are presented in Figures 4–6 and Figure S6 of the OSM.

The use of secondary raw materials affected the phase assemblage, formation kinetics and composition of the resulting hydrates. They influenced belite and ferrite hydration significantly for 5°C curing, but their effects diminished at higher temperatures. This is evident in the variations of strätlingite and the amorphous calcium silicate hydrate (C-S-H) phase, which form during belite hydration. In contrast, ye'elimite hydration was less affected across the different temperatures, as changes in the quantities of ettringite and monosulfate were less pronounced. While the enhanced early hydration and phase development can be largely attributed to higher mayenite content, other minor phases such as alkali sulfates and periclase may have also contributed to the observed differences.

With curing at 5°C, after 1 day of hydration, all the mixtures consumed nearly all ye'elimite and gypsum, resulting in substantial ettringite and, after the depletion of gypsum, the formation of monosulfate. A greater amount of monosulfate was observed in RMD, suggesting that the early reactions were faster in this mixture due to the higher mayenite content (Bullerjahn *et al*., 2019a;

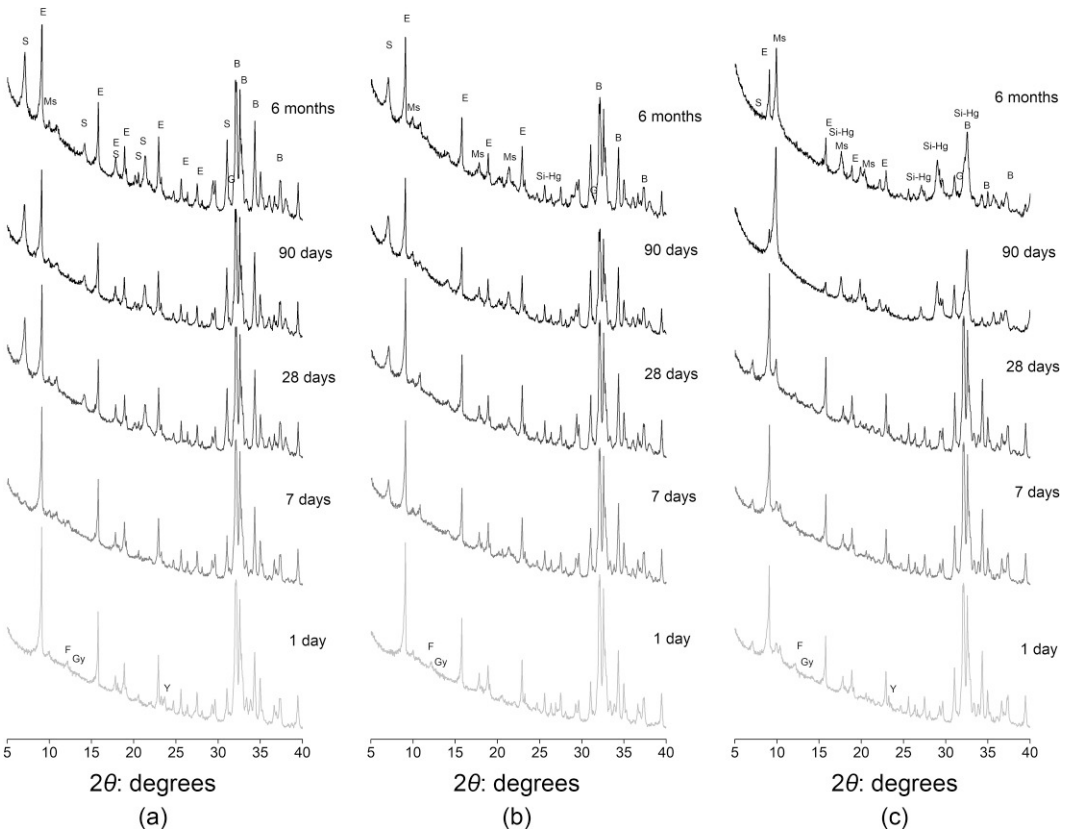

Figure 2. XRD patterns of NAT at different curing times and temperatures: (a) 5°C; (b) 20°C; (c) 60°C (B = belite, E = ettringite, F = ferrite, G = gehlenite, Gy = gypsum, Ms = monosulfate, S = strätlingite, Si-Hg = siliceous hydrogarnet, Y = ye'elimite)

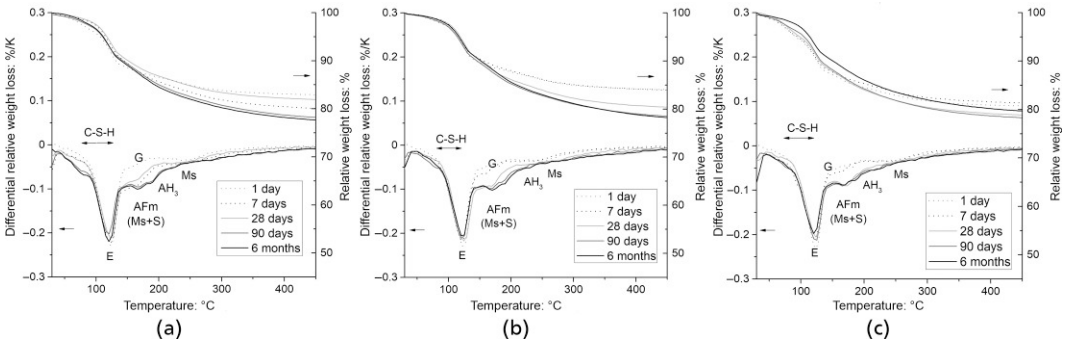

Figure 3. TGA of cement pastes cured at 20°C at different curing times: (a) NAT; (b) CON; (c) RMD (AH_3 = aluminium hydroxide, E = ettringite, G = gypsum, Ms = monosulfate, S = strätlingite)

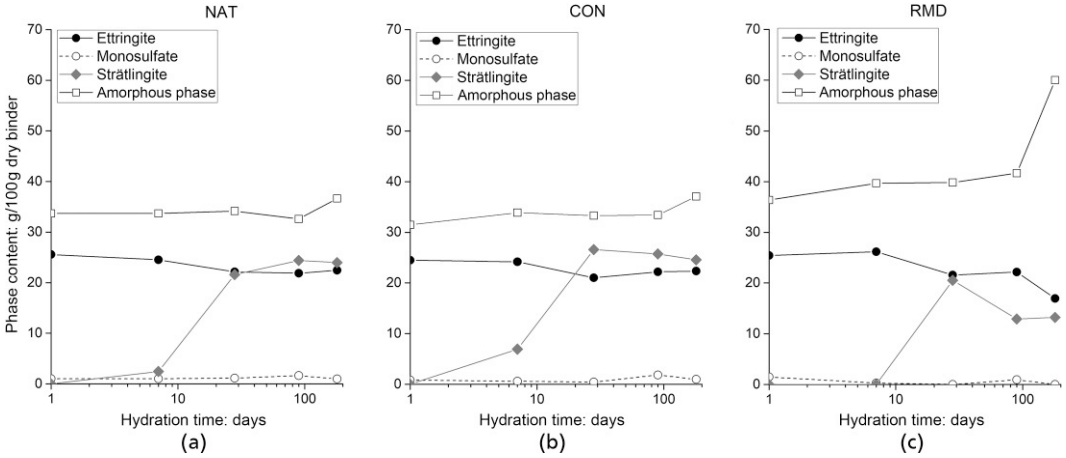

Figure 4. Comparison of the amount of hydration products formed in the NAT, CON and RMD cement mixtures at 5°C, as determined by quantitative XRD

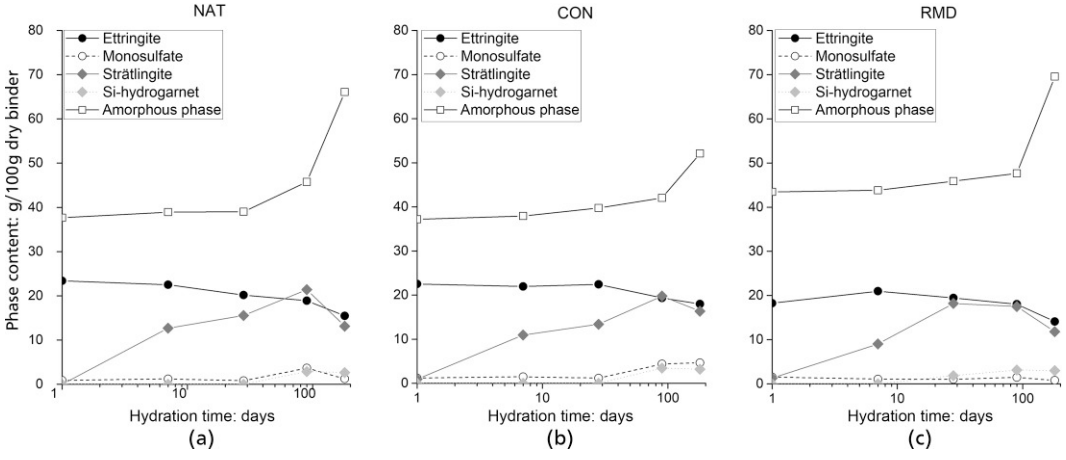

Figure 5. Comparison of the amount of hydration products formed in the NAT, CON and RMD cement mixtures at 20°C, as determined by quantitative XRD

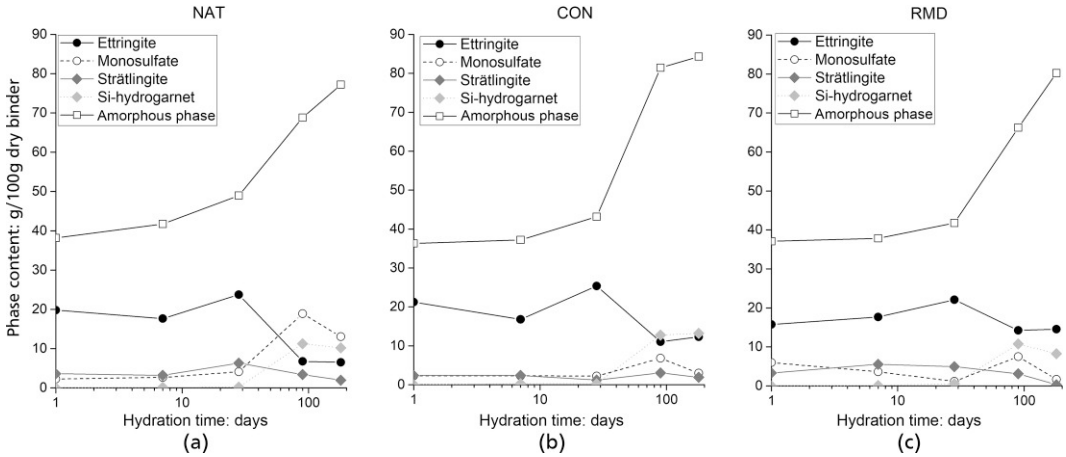

Figure 6. Comparison of the amount of hydration products formed in the NAT, CON and RMD cement mixtures at 60°C, as determined by quantitative XRD

Koehler *et al*., 2022), while CON displayed the smallest amount of monosulfate. The hydration of ettringite and gypsum also produced aluminium hydroxide, as confirmed by TGA through the weight loss near 250–280°C (Scrivener *et al*., 2016). This was later consumed during belite hydration to form strätlingite. Verifying C-S-H through XRD is difficult because it is amorphous, while TGA is also complicated as its primary water loss peak coincides with that of ettringite (Zajac *et al*., 2019). However, RMD consistently showed higher belite reaction degrees and amorphous content than NAT and CON at 5°C, likely due to its higher alkali sulfate content (Ma and Qian, 2018). These results suggest they contribute to a higher ionic strength and alkalinity in the pore solution, which promotes the dissolution of belite and enhances the precipitation of amorphous C-S-H gels. Also, alkali sulfates are known to shorten the induction period and enhance the acceleration phase of hydration, as also observed in the calorimetric data. This leads to faster nucleation and growth of hydration products, particularly C-S-H, at early ages. Moreover, aphthitalite has been reported to inhibit early ettringite formation but promote the transition to the acceleration phase more rapidly, potentially increasing the early precipitation of amorphous hydrates like C-S-H. This also suggests favoured C-S-H formation over strätlingite, as RMD contained less strätlingite and more amorphous material. The ferrite content decreased slowly, with nearly complete consumption after 90 days. In RMD, the reaction of ferrite was, at the beginning slower, than in NAT and CON, likely due to the higher content of alkali sulfates in RMD, which delay the hydration of ferrite (Morin *et al*., 2017). No siliceous hydrogarnet was observed in the cements cured at 5°C, as its formation is promoted by elevated temperatures (Dilnesa *et al*., 2014; Wang *et al*., 2017).

At 20°C, ye'elimite was depleted within 1 day, and gypsum remained only in traces. From 7 to 90 days, the amount of ettringite decreased while the amount of monosulfate continued to rise over time, attributed to the continuous hydration of the ferrite and the release of additional aluminium ions (Odler and Wonnemann, 1983; Taylor, 1997). These findings align with the TGA results, with weight loss near 120°C attributed to ettringite and that around 280°C to monosulfate (Andersen *et al*., 2004; Sáez del Bosque *et al*., 2014). At 1 day, RMD contained less ettringite, possibly due to aphthitalite inhibiting early ettringite formation (Sun *et al*., 2018), but had higher monosulfate levels due to accelerated reactions from increased mayenite content. A higher curing temperature reduced the amount of ettringite and increased the monosulfate content, consistent with the higher solubility of ettringite at elevated temperatures (Lothenbach *et al*., 2008; Wang *et al*., 2017). Strätlingite appeared at 1 day after curing at 20°C. RMD showed higher belite reaction degrees and amorphous content, again attributed to alkali sulfates. By 90 days, the ferrite was fully consumed. Ferrite hydration in RMD was slower in the early stages, consistent with the observations at 5°C, likely due to the alkali sulfates. Furthermore, the hydration of ferrite and belite led to the formation of siliceous hydrogarnet, which was higher in RMD cured at 20°C, where also the degree of belite hydration was higher.

At 60°C, ye'elimite and gypsum were depleted by 1 day. The trends in ettringite and monosulfate mirrored those at lower temperatures but were more pronounced; ettringite levels declined significantly between 7 and 90 days, while monosulfate levels steadily increased. Strätlingite appeared at 1 day, although its quantity decreased with temperature, as also noted by Mrak *et al*. (2024). RMD showed the highest belite reaction degrees and amorphous content at 60°C across all hydration times. Ferrite was fully consumed by 90 days. The ferrite content changed minimally up to 28 days, then dropped sharply to nearly zero. Siliceous hydrogarnet was present after 7 days of hydration; at late ages, it was highest in the CON mixture, where a higher degree of belite

hydration was also noted. Compared with curing at 20°C, more siliceous hydrogarnet precipitated at 60°C.

The influence of temperature on the hydration of cements was evident and the results confirm the findings in a previous study Mrak *et al*. (2024). Higher temperatures accelerated the hydration of anhydrous phases, as observed in NAT, CON and RMD. With an increase in curing temperature, ettringite solubility is higher, leading to a lower amount of ettringite, as also observed by Borštnar *et al*. (2020), favouring the formation of monosulfate (Kaufmann *et al*., 2016; Lothenbach *et al*., 2007). The strätlingite content decreased with increased temperatures after 28 days of hydration, regardless of the secondary raw material, coinciding with the formation of siliceous hydrogarnet, particularly at 60°C (Álvarez-Pinazo *et al*., 2016). At higher temperatures, increased amounts of siliceous hydrogarnet formed due to both the significantly higher degree of belite hydration (accompanied by greater amounts of C-S-H) and kinetic factors that further promote its development (Dilnesa *et al*., 2014; Wang *et al*., 2017).

NMR results

To confirm the presence of the amorphous phases (e.g. C-S-H or calcium aluminium silicate hydrate (C-(A)-S-H)) that could not be unambiguously determined by XRD and TGA, NMR was employed for NAT at 90 days of hydration. The results are shown in Figure 7.

As shown in Figure 7(a), ^{27}Al NMR confirmed the presence of ettringite and monosulfate, with chemical shifts at 14.5 ppm and 11.5 ppm, respectively (Le Saoût *et al*., 2013; Paul *et al*., 2015). Ettringite decreased with increasing curing temperature, while monosulfate increased, aligning with the XRD and TGA results. A narrow resonance for strätlingite at 62.5 ppm was observed at all temperatures, decreasing with temperature (Paul *et al*., 2015).

The presence of C-S-H was confirmed at all temperatures by ^{29}Si NMR (Figure 7(b)), with chemical shifts at −79 ppm and −84 ppm (Andersen *et al*., 2004; Le Saoût *et al*., 2013). These resonances decreased at a lower temperature, whereas the resonances of belite at around 71 ppm (Le Saoût *et al*., 2013) were increased, due to a lower degree of hydration. A signal at around 73.5 ppm is associated with non-reacted γ-C_2S (Sáez del Bosque *et al*., 2014). No C-S-H with incorporated aluminium was observed at 5°C using ^{27}Al NMR. At 60°C, a signal in the ^{27}Al NMR spectrum at around 75 ppm (associated with C-A-S-H) was detected, due to the partial substitution of silicon with aluminium in the bridging sites linking dimers of silicate tetrahedra (Avet *et al*., 2019; Thomas *et al*., 2003). At elevated temperatures, C-S-H exhibits a longer average chain length, a higher uptake of aluminium from the solution to bridging sites of C-A-S-H phase and a higher aluminium/silicon ratio (Bach *et al*., 2012; Thomas *et al*., 2003). When the aluminium/silicon ratio is 0.05 or less, most of the aluminium is incorporated into C-S-H. However, with a higher aluminium/silicon, the formation of strätlingite and/or katoite restricts the aluminium/silicon ratio in C-S-H to approximately 0.15, irrespective of the calcium/silicon ratio (L'Hôpital *et al*., 2016). The increase in the chain length of C-S-H at higher temperatures may result in a denser microstructure, which could lead to higher compressive strength (Sáez del Bosque *et al*., 2014). This is especially significant for mixtures where higher aluminium incorporation occurs, as C-A-S-H phases are typically associated with improved mechanical properties (Avet *et al*., 2019; Thomas *et al*., 2003). Temperature control during hydration allows tailoring specific phases to optimise durability and mechanical properties.

TEM results

TEM was used to investigate the morphology and chemical composition of hydrate assemblage in NAT after 90 days of hydration at temperatures of 5, 20 and 60°C (Figure 8, Table 4).

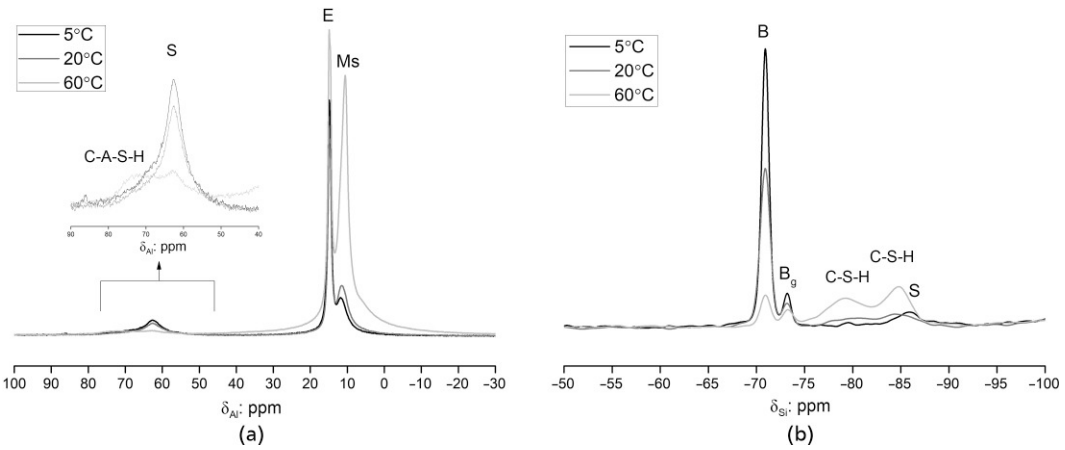

Figure 7. (a) ^{27}Al NMR and (b) ^{29}Si NMR analysis of NAT cement after 90 days of curing at different temperatures (B = belite, Bg = belite gamma, E = ettringite, Ms = monosulfate, S = strätlingite)

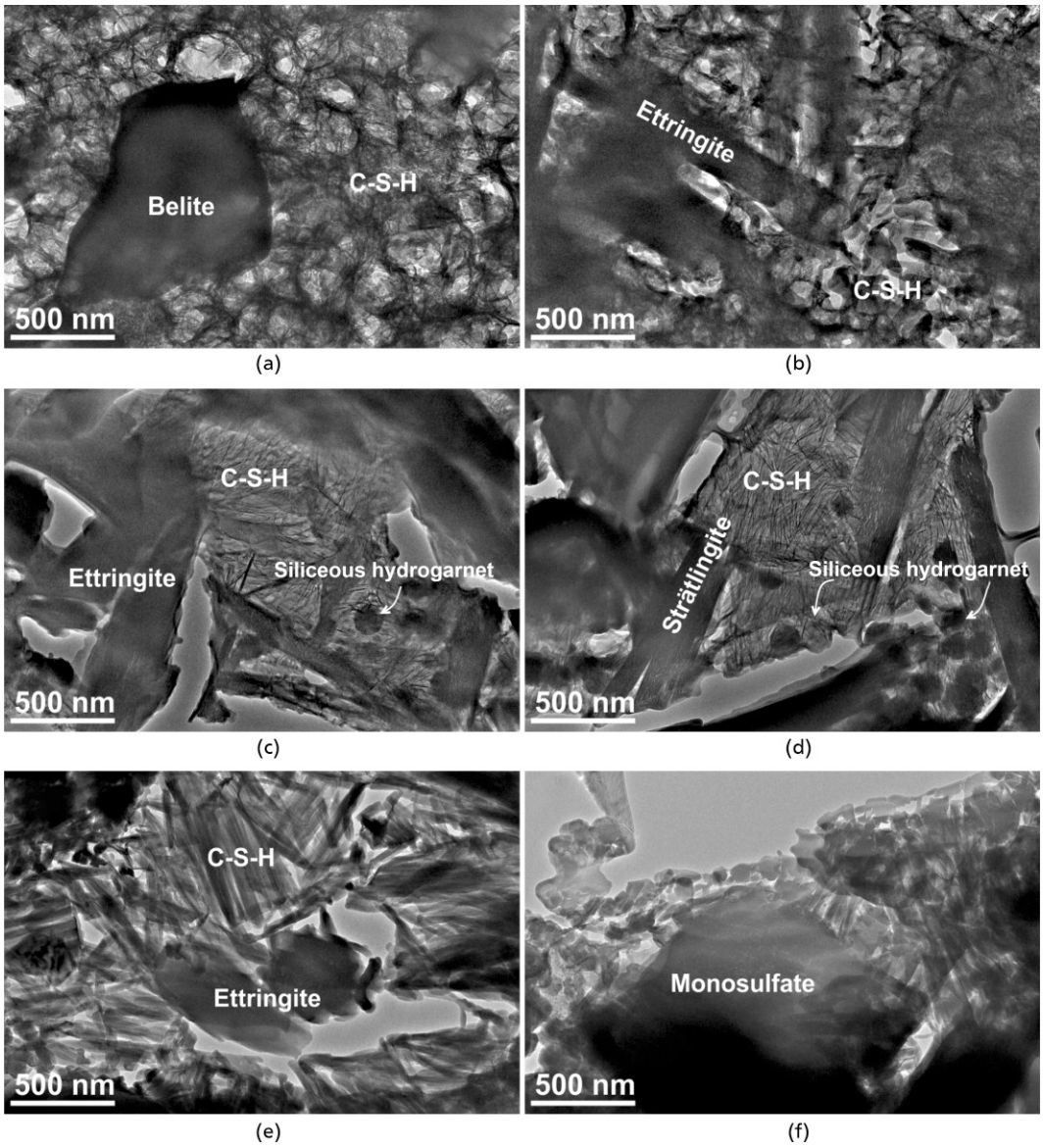

Figure 8. TEM micrographs of NAT after 90 days of hydration at different temperatures. (a) 5°C – a large grain of belite, surrounded by C-S-H. (b) 5°C – ettringite showing elongated morphology and fibrillar C-S-H. (c) 20°C – round grains of siliceous hydrogarnet, long rods of strätlingite and large plates of ettringite. (d) 20°C – C-S-H surrounding other hydration products. (e) 60°C – large grains of ettringite and monosulfate. (f) 60°C –C-S-H and siliceous hydrogarnet intermixed

At 5°C, the cement microstructure was more homogenous, which is related to slower hydration (De Weerdt *et al*., 2012; Myers *et al*., 2015). At 5°C and 20°C, remaining unhydrated belite grains were common, but scarce at 60°C, as the degree of hydration is higher at elevated temperatures. EDXS analysis confirmed presence of ettringite, monosulfate, strätlingite and C-S-H at all temperatures. Siliceous hydrogarnet appeared at 20°C and 60°C, consistent with the XRD and TGA results.

Ettringite formed large elongated particles, with grain size decreasing as the curing temperature increased due to accelerated hydration of ye'elimite (Borštnar *et al*., 2020; Lothenbach *et al*., 2007). The largest amounts of ettringite were for the samples cured at 5°C and 20°C, aligning with the XRD data. The ettringite composition was stable across temperatures, containing small amounts of iron, silicon and potassium. In ettringite, aluminium can be substituted by iron, calcium, sulfate and silicon, while sulfate can be replaced with selenium or chromium (Lukas, 1976; Möschner *et al*., 2009). Iron-rich ettringite forms more slowly than aluminium-ettringite, but higher temperatures reduce this disparity (Möschner *et al*., 2009). Small amounts of iron were detected in the ettringite at all temperatures. Borštnar *et al*. (2020) reported that ettringite shows the ability for higher ion uptake at elevated temperatures.

Table 4. Chemical composition of hydration phases determined by TEM/EDXS. Compositions were calculated to all elements and only cations were considered in the calculations. Hydrogarnet was not detected at 5°C

	Composition: at.%					
Phase	Al K	Si K	S K	K K	Ca K	Fe K
90 days, 5°C						
Ettringite	16.1	3.7	26.1	1.5	50.5	0.9
Strätlingite	34.1	17.5	1.1	1.9	41.3	3.6
Hydrogarnet	ND[a]	ND	ND	ND	ND	ND
C-S-H	6.3	30.2	4.6	2.6	50.7	5.4
90 days, 20°C						
Ettringite	17.8	1.5	26.5	1.4	52.3	0.4
Strätlingite	32.7	17.7	2.2	1.5	42.3	3.4
Hydrogarnet	11.3	23.1	2.0	0.9	52.8	8.8
C-S-H	6.8	31.2	2.8	1.7	55.4	1.3
90 days, 60°C						
Ettringite	17.3	2.3	25.8	1.0	53.4	0.4
Monosulfate	22.9	3.7	12.9	BD[b]	58.8	1.1
Hydrogarnet	15.2	21.7	3.3	BD	54.8	3.2
C-S-H	3.2	20.9	2.9	1.3	60.7	0.4

[a]Not detected
[b]Below detection limit

Monosulfate was observed by TEM only at 60°C, forming plate-like grains with irregular morphology, incorporating small amounts of silicon and iron (Dilnesa *et al*., 2012; Mathur, 2007; Richardson *et al*., 2010). In monosulfate, the substitution of different anions such as OH^-, SO_4^{2-}, CO_3^{2-} and Cl^- has been reported, and the replacement of aluminium by iron, resulting in iron-monosulfate formation (Dilnesa *et al*., 2012).

Strätlingite was found as elongated grains with a laminar structure, precipitating more abundantly at 5°C and 20°C. It contained up to 3.4 at.% iron, with minor changes in composition across temperatures. Iron-rich strätlingite forms due to partial aluminium replacement by iron (Álvarez-Pinazo *et al*., 2013; Wang, 2011).

Siliceous hydrogarnet occurs in the form of spherical grains with a diameter of around 100 nm. The grains are usually found in cubic form, but were rapidly amorphised during the TEM observation, indicating that it is sensitive to high-energy electrons. While siliceous hydrogarnet grains were not observed at 5°C (Dilnesa *et al*., 2014), they increased with an increase in curing temperature (Mrak *et al*., 2024). It contains up to 10 at.% of iron. The amount of iron is much higher at 20°C compared with 60°C, while the amount of aluminium is slightly lower. In Portland cements, iron and aluminium intermixed with siliceous hydrogarnet are usually observed (Taylor and Newbury, 1984). The hydrogarnet structure can be changed by the replacement of all or part of the silicon atoms and a solid solution between C_3AH_6, C_3FH_6, C_3AS and C_3FS_3 exists (Dilnesa *et al*., 2014; Taylor, 1990). Thermodynamic modelling of BYF cement (Mrak *et al*., 2024) indicates that iron is incorporated in siliceous hydrogarnet, which is a result of partial replacement of aluminium ions by iron, forming iron-rich siliceous hydrogarnet (Álvarez-Pinazo *et al*., 2013).

The C-S-H showed a fibrillar morphology at 5°C, transitioning to foil-like structures at elevated temperatures, where it intermixed with siliceous hydrogarnet. A recent investigation on iron incorporation in C-S-H showed that C-S-H with less iron shows foil-like morphology (Siramanont *et al*., 2021). While NMR revealed the incorporation of aluminium in the C-S-H structure at 60°C, the amount of aluminium was not high according to the TEM results, probably due to intermixing with other phases. Previous studies on C-S-H in ordinary Portland cement at different temperatures also showed a slight increase in sulfur and aluminium at elevated temperatures (Gallucci *et al*., 2013; Sáez del Bosque *et al*., 2014). The observed differences in phase assemblage and microstructure among the mixtures emphasise the importance of controlling the secondary raw material composition to optimise cement properties.

Compressive strength

Figure 9 shows the effects of the different secondary raw materials on the development of compressive strength for curing temperatures of 5, 20 and 60°C. The early strength development was similar across all mixtures but diverged after 28 days. Fast early

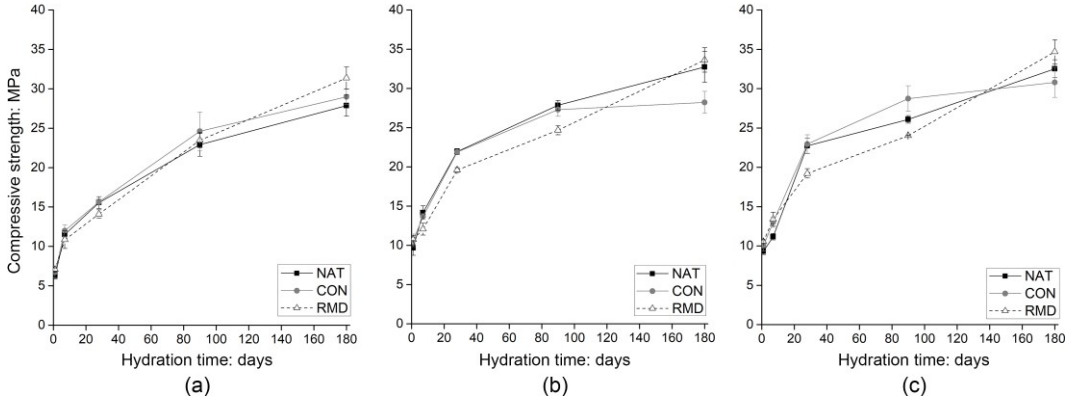

Figure 9. Development of compressive strength in NAT, CON and RMD at different curing temperatures: (a) 5°C; (b) 20°C; (c) 60°C

strength development was displayed at all curing temperatures due to the quick reaction of ye'elimite and gypsum with water, resulting in the formation of ettringite, which plays a substantial role in contributing to the early strength of cements (Jeong *et al*., 2018; Lothenbach *et al*., 2015). At 1 day, the lowest strength was observed for 5°C curing, attributed to residual gypsum.

At 20°C and 60°C, RMD exhibited lower compressive strength than NAT and CON (up to 90 days of hydration), consistent with earlier studies (Ma and Qian, 2018; Sun *et al*., 2018). This may be linked to the presence of mayenite, which, as reported by He and Li (2018), reduces strength after 14–28 days by forming AFm phases and lowering the AFt/AFm ratio.

After curing at 20°C and 60°C for 180 days, RMD demonstrated slightly higher strength, while CON showed the lowest strength. This strength reduction could be due to the higher periclase content in the CON mixture. Mo *et al*. (2015) found that mortars incorporating magnesium oxide exhibit reduced compressive strength due to the higher water consumption caused by the magnesium oxide reaction and the formation of magnesium hydroxide, which lead to expansion, the creation of cracks and increased porosity (Ali and Mullick, 1998; Wang *et al*., 2022).

Figure 9 also shows that all the compressive strengths at late ages (i.e. 6 months) increased with an increase in curing temperature. This is because belite hydration is enhanced, leading to the precipitation of strätlingite, C-S-H and siliceous hydrogarnet, which fill more space, as shown by Mrak *et al*. (2024) and others (Shirani *et al*., 2021; Sui *et al*., 2015). However, the high mayenite content from the red mud reduced the strength at higher temperatures, and the waste concrete's higher periclase content led to lower strength at elevated temperatures.

MIP

The effect of secondary raw materials on the porosity of the cements at 90 days (measured by MIP) is shown in Figure 10. After curing at 5°C and 60°C, the pore sizes exhibited a unimodal distribution, with main peaks around 0.07 µm. At 20°C, the intrusion peak shifted to around 0.02 µm. At 5°C, another intrusion peak was observed in RMD at around 0.25 µm, leading to a bimodal distribution and suggesting larger pores due to the formation of less monosulfate and strätlingite and more C-S-H that fill smaller pores in RMD compared with NAT and CON. A higher degree of hydration leads to more hydration products, which makes the microstructure more heterogeneous (Li *et al*., 2019; Wang *et al*., 2017).

The median and average pore diameters were higher for the 5°C samples than the 20°C and 60°C samples, corresponding to fewer hydration products forming at lower hydration degrees. No significant correlation was observed between the incorporation of secondary raw materials and the pore size distribution.

Table 5 shows higher porosity in RMD compared with NAT and CON at 5°C and 60°C, likely due to the higher degree of reaction in RMD. Porosity increased in the samples cured at 60°C compared with 5°C and 20°C, consistent with findings that lower temperatures promote a denser, more uniform matrix due to slower hydration (Li *et al*., 2019; Wang *et al*., 2017; Xu *et al*., 2018). The negative correlation between compressive strength and porosity is evident. For curing at 20°C, the lowest porosity coincided with the highest compressive strength. These findings show that secondary raw materials significantly influence porosity and strength development through their impact on the distribution and microstructure of the hydration assemblage.

Conclusions

The introduction of different raw materials that lead to changes in the amounts of minor phases in BYF cement clinker was studied. The incorporation of red mud accelerated the early hydration at low temperatures, as this cement had higher contents of mayenite and alkali sulfate. Waste concrete slowed hydration due to its lower

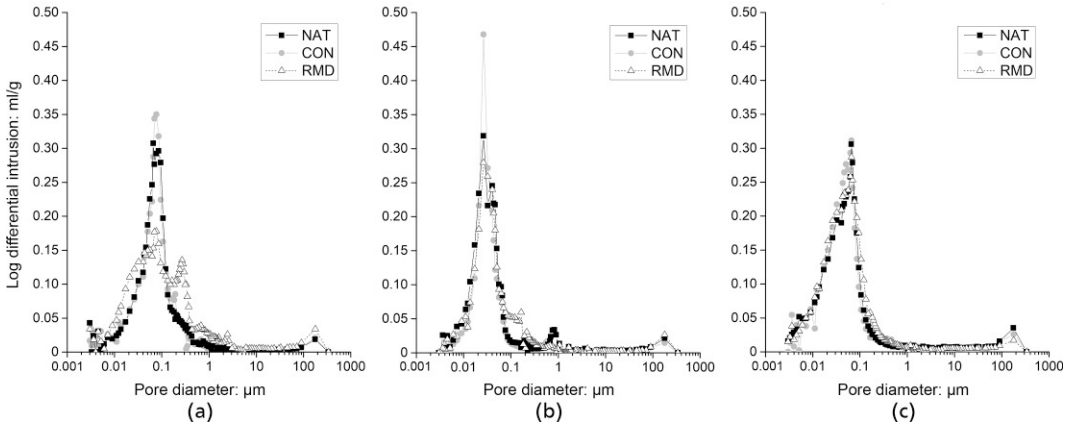

Figure 10. Plots of log differential intrusion against pore diameter of the NAT, CON and RMD cement samples after 90 days of hydration at: (a) 5°C; (b) 20°C; (c) 60°C

Table 5. Porosity and pore size distribution after 90 days of hydration (measured by MIP)

	Temperature 5°C			Temperature 20°C			Temperature 60°C		
	NAT	CON	RMD	NAT	CON	RMD	NAT	CON	RMD
Porosity: %	31.82	31.79	35.50	29.63	27.50	29.02	35.69	34.29	37.29
Median pore diameter: µm	0.078	0.077	0.087	0.032	0.032	0.037	0.051	0.048	0.051
Average pore diameter: µm	0.041	0.041	0.039	0.026	0.030	0.030	0.027	0.029	0.029
Bulk density: g/ml	1.57	1.56	1.51	1.58	1.63	1.59	1.50	1.50	1.50
Apparent density: g/ml	2.31	2.29	2.34	2.24	2.25	2.24	2.34	2.28	2.39

mayenite content and slower reaction kinetics. These effects were more pronounced for curing at 5°C, particularly during belite hydration, influencing strätlingite levels and C-S-H formation. Ye'elimite hydration was less affected, with minor changes in ettringite and monosulfate levels. The early formation of ettringite was slightly inhibited in the cement with red mud because of the increased presence of aphthitalite, while a higher amount of monosulfate formed as a result of the greater mayenite content, which accelerated the hydration of ye'elimite. Red mud delayed ferrite hydration, due to the greater presence of alkali sulfate in the cement clinker, which enhanced belite reactivity, reduced strätlingite and increased C-S-H. This indicates that – in the presence of a higher alkali sulfate content – a predominant transformation of belite into C-S-H rather than strätlingite occurs. Waste concrete increased the formation of siliceous hydrogarnet at higher temperatures, contributing to delayed but stable strength development due to higher periclase content in the cement clinker and altering the overall phase assemblage, including a higher degree of belite hydration. NMR analysis showed greater aluminium incorporation into C-A-S-H at elevated temperatures, enhancing strength and durability by forming stable phases like C-A-S-H and monosulfate.

These findings contribute to broader understanding of how industrial residues influence cement hydration mechanisms and material properties at different curing temperatures. Importantly, the research highlights the potential of BYF cements to address critical environmental challenges by providing a sustainable alternative to ordinary Portland cement. Future work should explore the scalability of these findings and investigate long-term durability in real-world applications to further promote the adoption of these eco-friendly materials.

Acknowledgements

The research was performed within the Young Researcher Programme and was financially supported by the Slovenian Research Agency, contract number 1000-18-1502.

REFERENCES

Akhtar A and Sarmah AK (2018) Construction and demolition waste generation and properties of recycled aggregate concrete: a global perspective. *Journal of Cleaner Production* **186**: 262–281, 10.1016/j.jclepro.2018.03.085.

Ali MM and Mullick AK (1998) Volume stabilisation of high MgO cement: effect of curing conditions and fly ash addition. *Cement and Concrete Research* **28(11)**: 1585–1594, 10.1016/S0008-8846(98)00140-9.

Álvarez-Pinazo G, Santacruz I, León-Reina L, Aranda MAG and De la Torre AG (2013) Hydration reactions and mechanical strength developments of iron-rich sulfobelite eco-cements. *Industrial & Engineering Chemistry Research* **52(47)**: 16606–16614, 10.1021/ie402484e.

Álvarez-Pinazo G, Santacruz I, Aranda MAG and De la Torre ÁG (2016) Hydration of belite–ye'elimite–ferrite cements with different calcium sulfate sources. *Advances in Cement Research* **28(8)**: 529–543.

Andersen MD, Jakobsen HJ and Skibsted J (2004) Characterization of white Portland cement hydration and the C-S-H structure in the presence of sodium aluminate by ^{27}Al and ^{29}Si MAS NMR spectroscopy. *Cement and Concrete Research* **34(5)**: 857–868, 10.1016/j.cemconres.2003.10.009.

Avet F, Boehm-Courjault E and Scrivener K (2019) Investigation of C-A-S-H composition, morphology and density in limestone calcined clay cement (LC3). *Cement and Concrete Research* **115**: 70–79, 10.1016/j.cemconres.2018.10.011.

Bach TTH, Coumes CCD, Pochard I *et al.* (2012) Influence of temperature on the hydration products of low pH cements. *Cement and Concrete Research* **42(6)**: 805–817, 10.1016/j.cemconres.2012.03.009.

Baltakys K, Dambrauskas T, Rubinaite D, Siauciunas R and Grineviciene A (2021) Formation and hydration of eco-friendly cement using industrial wastes as raw materials. *Scientific Reports* **11(1)**: 14742, 10.1038/s41598-021-94148-x.

Borštnar M, Daneu N and Dolenec S (2020) Phase development and hydration kinetics of belite-calcium sulfoaluminate cements at different curing temperatures. *Ceramics International* **46(18)**: 29421–29428.

BSI (2013) BS EN 196-2:2013: Method of testing cement – Chemical analysis of cement. BSI, London, UK.

Bullerjahn F, Zajac M and Ben Haha M (2015) CSA raw mix design: effect on clinker formation and reactivity. *Materials and Structures* **48(12)**: 3895–3911, 10.1617/s11527-014-0451-z.

Bullerjahn F, Zajac M, Ben Haha M and Scrivener KL (2019a) Factors influencing the hydration kinetics of ye'elimite; effect of mayenite. *Cement and Concrete Research* **116**: 113–119, 10.1016/j.cemconres.2018.10.026.

Bullerjahn F, Boehm-Courjault E, Zajac M, Ben Haha M and Scrivener K (2019b) Hydration reactions and stages of clinker composed mainly of stoichiometric ye'elimite. *Cement and Concrete Research* **116**: 120–133, 10.1016/j.cemconres.2018.10.023.

Chen IA and Juenger MCG (2011) Synthesis and hydration of calcium sulfoaluminate-belite cements with varied phase compositions. *Journal of Materials Science* **46(8)**: 2568–2577.

Chitvoranund N (2021) *Stability of Hydrate Assemblages and Properties of Cementitious Systems with Higher Alumina Content*. EPFL, Lausanne, Switzerland.

Cuesta A, De la Torre AG, Losilla ER *et al.* (2013) Structure, atomistic simulations, and phase transition of stoichiometric yeelimite. *Chemistry of Materials* **25(9)**: 1680–1687, 10.1021/cm400129z.

Cuesta A, De la Torre ÁG, Losilla ER, Santacruz I and Aranda MAG (2014) Pseudocubic crystal structure and phase transition in doped ye'elimite. *Crystal Growth & Design* **14(10)**: 5158–5163.

De Souza VCG, Koppe JC, Costa JFCL *et al.* (2008) The influence of mineralogical, chemical and physical properties on grindability of commercial clinkers with high MgO level. *Cement and Concrete Research* **38(8–9)**: 1119–1125, 10.1016/j.cemconres.2008.02.011.

De Weerdt K, Ben Haha M, Le Saout G *et al.* (2012) The effect of temperature on the hydration of composite cements containing limestone powder and fly ash. *Materials and Structures* **45(7)**: 1101–1114, 10.1617/s11527-011-9819-5.

Dilnesa BZ, Lothenbach B, Renaudin G, Wichser A and Wieland E (2012) Stability of monosulfate in the presence of iron. *Journal of the American Ceramic Society* **95(10)**: 3305–3316, 10.1111/j.1551-2916.2012.05335.x.

Dilnesa BZ, Lothenbach B, Renaudin G, Wichser A and Kulik D (2014) Synthesis and characterization of hydrogarnet $Ca_3(Al_xFe_{1-x})_2(SiO_4)_y(OH)_{4(3-y)}$. *Cement and Concrete Research* **59**: 96–111, 10.1016/j.cemconres.2014.02.001.

Dolenec S, Šter K, Borštnar M *et al.* (2020) Effect of the cooling regime on the mineralogy and reactivity of belite-sulfoaluminate clinkers. *Minerals* **10(10)**: 910, 10.3390/min10100910.

Edmonds RN and Majumdar AJ (1988) The hydration of $12CaO.7A1_2O_3$ at different temperatures. *Cement and Concrete Research* **18(3)**: 473–478, 10.1016/0008-8846(88)90082-8.

Galbenis C-T and Tsimas S (2006) Use of construction and demolition wastes as raw materials in cement clinker production. *China Particuology* **4(2)**: 83–85, 10.1016/S1672-2515(07)60241-3.

Gallucci E, Zhang X and Scrivener KL (2013) Effect of temperature on the microstructure of calcium silicate hydrate (C-S-H). *Cement and Concrete Research* **53**: 185–195.

Gartner E (2017) What are BYF cements, and how do they differ from CSA cements? In *The Future of Cement, 200 years after Louis Vicat, UNESCO, Paris, France*.

Gastaldi D, Canonico F, Capelli L *et al.* (2015) An investigation on the recycling of hydrated cement from concrete demolition waste. *Cement & Concrete Composites* **61**: 29–35, 10.1016/j.cemconcomp.2015.04.010.

He Z and Li Y (2018) The influence of mayenite employed as a functional component on hydration properties of ordinary Portland cement. *Materials* **11(10)**: 1958, 10.3390/ma11101958.

Huang L, Song W, Li H, Zhang H and Yang Z (2018) Effects of aphthitalite on the formation of clinker minerals and hydration properties. *Construction and Building Materials* **183**: 275–282, 10.1016/j.conbuildmat.2018.06.082.

Jansen D, Goetz-Neunhoeffer F, Stabler C and Neubauer J (2011) A remastered external standard method applied to the quantification of early OPC hydration. *Cement and Concrete Research* **41(6)**: 602–608.

Jeong Y, Hargis CW, Chun S-C and Moon J (2018) The effect of water and gypsum content on strätlingite formation in calcium sulfoaluminate-belite cement pastes. *Construction and Building Materials* **166**: 712–722.

Jun Y, Kim JH and Kim T (2019) Hydration of calcium sulfoaluminate-based binder incorporating red mud and silica fume. *Applied Sciences* **9(11)**: 2270, 10.3390/app9112270.

Kaufmann J, Winnefeld F and Lothenbach B (2016) Stability of ettringite in CSA cement at elevated temperatures. *Advances in Cement Research* **28(4)**: 251–261.

Koehler A, Neubauer J and Goetz-Neunhoeffer F (2022) How $C_{12}A7$ influences the early hydration of calcium aluminate cement at different temperatures. *Cement and Concrete Research* **162**: 106972, 10.1016/j.cemconres.2022.106972.

Koplík J, Tomala L and Novotný R (2014) Hydration of calcium aluminate phases at different temperatures. *Advanced Materials Research* **1000**: 24–27, 10.4028/www.scientific.net/AMR.1000.24.

Kou S, Poon C and Agrela F (2011) Comparisons of natural and recycled aggregate concretes prepared with the addition of different mineral admixtures. *Cement & Concrete Composites* **33(8)**: 788–795, 10.1016/j.cemconcomp.2011.05.009.

Kumar S and Kameswara Rao CVS (1994) Effect of sulfates on the setting time of cement and strength of concrete. *Cement and Concrete Research* **24(7)**: 1237–1244, 10.1016/0008-8846(94)90108-2.

Kurdowski W (2014) *Cement and Concrete Chemistry*. Springer, Dordrecht, the Netherlands.

L'Hôpital E, Lothenbach B, Kulik DA and Scrivener K (2016) Influence of calcium to silica ratio on aluminium uptake in calcium silicate hydrate. *Cement and Concrete Research* **85**: 111–121, 10.1016/j.cemconres.2016.01.014.

Le Saoût G, Lothenbach B, Hori A, Higuchi T and Winnefeld F (2013) Hydration of Portland cement with additions of calcium sulfoaluminates. *Cement and Concrete Research* **43**: 81–94, 10.1016/j.cemconres.2012.10.011.

Li L, Wang R and Zhang S (2019) Effect of curing temperature and relative humidity on the hydrates and porosity of calcium sulfoaluminate cement. *Construction and Building Materials* **213**: 627–636.

Liu GQ, Yang QX, Jiang L *et al.* (2017) Sintering characteristics of BCSAF cement clinker with added wastes from production of manganese and magnesium metals. *Advances in Cement Research* **29(6)**: 227–235.

Lothenbach B, Winnefeld F, Alder C, Wieland E and Lunk P (2007) Effect of temperature on the pore solution, microstructure and hydration products of Portland cement pastes. *Cement and Concrete Research* **37(4)**: 483–491.

Lothenbach B, Matschei T, Möschner G and Glasser FP (2008) Thermodynamic modelling of the effect of temperature on the hydration and porosity of Portland cement. *Cement and Concrete Research* **38(1)**: 1–18.

Lothenbach B, Albert B, Vincent M and Ellis G (2015) Hydration of belite-ye'elimite-ferrite cements: thermodynamic modeling. In *Proceedings of the 14th International Conference on the Chemistry of Cement, Beijing, China*.

Lothenbach B, Durdzinski P and De Weerdt K (2016) Thermogravimetric analysis. In *A Practical Guide to Microstructural Analysis of Cementitious Materials*. CRC Press, Boca Raton, FL, USA.

Lukas W (1976) Substitution of Si in the lattice of ettringite. *Cement and Concrete Research* **6(2)**: 225–233, 10.1016/0008-8846(76)90120-4.

Ma Y and Qian J (2018) Influence of alkali sulfates in clinker on the hydration and hardening of Portland cement. *Construction and Building Materials* **180**: 351–363, 10.1016/j.conbuildmat.2018.05.196.

Manfroi EP, Cheriaf M and Rocha JC (2014) Microstructure, mineralogy and environmental evaluation of cementitious composites produced with red mud waste. *Construction and Building Materials* **67**, 29–36, 10.1016/j.conbuildmat.2013.10.031.

Mathur PC (2007) *Study of Cementitious Materials Using Transmission Electron Microscopy*. PhD thesis, EPFL, Laussane, Switzerland.

Mo L, Liu M, Al-Tabbaa A and Deng M (2015) Deformation and mechanical properties of the expansive cements produced by inter-grinding cement clinker and MgOs with various reactivities. *Construction and Building Materials* **80**: 1–8, 10.1016/j.conbuildmat.2015.01.066.

Morin V, Termkhajornkit P, Huet B and Pham G (2017) Impact of quantity of anhydrite, water to binder ratio, fineness on kinetics and phase assemblage of belite-ye'elimite-ferrite cement. *Cement and Concrete Research* **99**: 8–17.

Möschner G, Lothenbach B, Winnefeld F *et al.* (2009) Solid solution between Al-ettringite and Fe-ettringite ($Ca_6[Al_{1-x}Fe_x(OH)_6]_2(SO_4)_3{\cdot}26H_2O$). *Cement and Concrete Research* **39(6)**: 482–489.

Mrak M, Winnefeld F, Lothenbach B and Dolenec S (2021) The influence of calcium sulfate content on the hydration of belite-calcium sulfoaluminate cements with different clinker phase compositions. *Materials and Structures* **54(6)**: 212.

Mrak M, Winnefeld F, Lothenbach B, Legat A and Dolenec S (2024) Experimental study and thermodynamic modelling of the temperature effect on the hydration of belite-ye'elimite-ferrite cements. *Construction and Building Materials* **411**: 134260, 10.1016/j.conbuildmat.2023.134260.

Myers RJ, L'Hôpital E, Provis JL and Lothenbach B (2015) Effect of temperature and aluminium on calcium (alumino)silicate hydrate chemistry under equilibrium conditions. *Cement and Concrete Research* **68**: 83–93, 10.1016/j.cemconres.2014.10.015.

O'Connor BH and Raven MD (1988) Application of the Rietveld refinement procedure in assaying powdered mixtures. *Powder Diffraction* **3**: 2–6.

Odler I and Wonnemann R (1983) Effect of alkalies on Portland cement hydration II. Alkalies present in form of sulphates. *Cement and Concrete Research* **13(6)**: 771–777, 10.1016/0008-8846(83)90078-9.

Oliveira TCF, Dezen BGS and Possan E (2020) Use of concrete fine fraction waste as a replacement of Portland cement. *Journal of Cleaner Production* **273**: 123126, 10.1016/j.jclepro.2020.123126.

Paul G, Boccaleri E, Buzzi L, Canonico F and Gastaldi D (2015) Friedel's salt formation in sulfoaluminate cements: a combined XRD and ^{27}Al MAS NMR study. *Cement and Concrete Research* **67**: 93–102, 10.1016/j.cemconres.2014.08.004.

Richardson IG, Skibsted J, Black L and Kirkpatrick RJ (2010) Characterisation of cement hydrate phases by TEM, NMR and Raman spectroscopy. *Advances in Cement Research* **22(4)**: 233–248, 10.1680/adcr.2010.22.4.233.

Sáez del Bosque IF, Martínez-Ramírez S, Martín-Pastor M and Blanco-Varela MT (2014) Effect of temperature on C–S–H gel nanostructure in white cement. *Materials and Structures* **47(11)**: 1867–1878, 10.1617/s11527-013-0156-8.

Samet B and Sarkar SL (1997) The influence of calcium sulfate form on the initial hydration of clinkers containing different alkali combinations. *Cement and Concrete Research* **27(3)**: 369–380, 10.1016/S0008-8846(97)00030-6.

Scrivener KL and Capmas A (1998) Calcium aluminate cements. In *Lea's Chemistry of Cement and Concrete*. Butterworth-Heinemann, pp. 713–782.

Scrivener K, Snellings R and Lothenbach B (2016) *A Practical Guide to Microstructural Analysis of Cementitious Materials*. CRC Press, Boca Raton, FL, USA.

Shirani S, Cuesta A, Morales-Cantero A *et al.* (2021) Influence of curing temperature on belite cement hydration: a comparative study with Portland cement. *Cement and Concrete Research* **147**: 106499, 10.1016/j.cemconres.2021.106499.

Siramanont J, Walder BJ, Emsley L and Bowen P (2021) Iron incorporation in synthetic precipitated calcium silicate hydrates. *Cement and Concrete Research* **142**: 106365, 10.1016/j.cemconres.2021.106365.

Snellings R (2013) Solution-controlled dissolution of supplementary cementitious material glasses at pH 13: the effect of solution composition on glass dissolution rates. *Journal of the American Ceramic Society* **96(8)**: 2467–2475, 10.1111/jace.12480.

Snellings R (2016) X-ray powder diffraction applied to cement. In *A Practical Guide to Microstructural Analysis of Cementitious Materials*. CRC Press, Boca Raton, FL, USA, pp. 126–195.

Snellings R, Chwast J, Cizer Ö *et al.* (2018) Report of TC 238-SCM: hydration stoppage methods for phase assemblage studies of blended cements—results of a round robin test. *Materials and Structures* **51(4)**: 111.

Sui T, Fan L, Wen Z and Wang J (2015) Properties of belite-rich Portland cement and concrete in China. *Journal of Civil Engineering and Architecture* **9**: 384–392, 10.17265/1934-7359/2015.04.002.

Sun H, Qian J, Xiong Q *et al.* (2018) Effects of alkali sulfates in clinker on hydration and hardening performance of Portland cement. *Advances in Cement Research* **30(4)**: 172–184, 10.1680/jadcr.17.00030.

Taylor HF (1990) *Cement Chemistry*. Academic Press, London, UK.

Taylor HFW and Newbury DE (1984) An electron microprobe study of a mature cement paste. *Cement and Concrete Research* **14(4)**: 565–573, 10.1016/0008-8846(84)90134-0.

Taylor HFW (1997) *Cement Chemistry*. Thomas Telford Publishing, London, UK.

Taylor HFW (1999) Distribution of sulfate between phases in Portland cement clinkers. *Cement and Concrete Research* **29(8)**: 1173–1179, 10.1016/S0008-8846(98)00241-5.

Telesca A, Marroccoli M and Winnefeld F (2019) Synthesis and characterisation of calcium sulfoaluminate cements produced by different chemical gypsums. *Advances in Cement Research* **31(3)**: 113–123, 10.1680/jadcr.18.00122.

Thomas JJ, Rothstein D, Jennings HM and Christensen BJ (2003) Effect of hydration temperature on the solubility behavior of Ca-, S-, Al-, and Si-bearing solid phases in Portland cement pastes. *Cement and Concrete Research* **33(12)**: 2037–2047, 10.1016/S0008-8846(03)00224-2.

Vangelatos I, Angelopoulos GN and Boufounos D (2009) Utilization of ferroalumina as raw material in the production of ordinary Portland cement. *Journal of Hazardous Materials* **168(1)**: 473–478, 10.1016/j.jhazmat.2009.02.049.

Wang J (2011) *Hydration Mechanism of Cements based on low-CO2 Clinkers containing Belite, Ye'elimite and Calcium Alumino-ferrite*. PhD thesis, Université Des Sciences et Technologie de Lille, Lille, France.

Wang C, Zhou Z, Liu C and Cheng X (2011) Formation kinetics of Portland cement clinker containing with magnesium oxide. *Journal of the Chinese Ceramic Society* **39**: 714–717.

Wang P, Li N and Xu L (2017) Hydration evolution and compressive strength of calcium sulphoaluminate cement constantly cured over the temperature range of 0 to 80°C. *Cement and Concrete Research* **100**: 203–213, 10.1016/j.cemconres.2017.05.025.

Wang L, Lu X, Liu L *et al.* (2022) Influence of MgO on the hydration and shrinkage behavior of low heat Portland cement-based materials via pore structural and fractal analysis. *Fractal and Fractional* **6(1)**: 40, 10.3390/fractalfract6010040.

Winnefeld F, Martin LHJ, Müller CJ and Lothenbach B (2017) Using gypsum to control hydration kinetics of CSA cements. *Construction and Building Materials* **155**: 154–163.

Xu L, Liu S, Li N *et al.* (2018) Retardation effect of elevated temperature on the setting of calcium sulfoaluminate cement clinker. *Construction and Building Materials* **178**: 112–119.

Zajac M, Skocek J, Stabler C, Bullerjahn F and Ben Haha M (2019) Hydration and performance evolution of belite-ye'elimite-ferrite cement. *Advances in Cement Research* **31(3)**: 124–137, 10.1680/jadcr.18.00110.

Zhang N, Liu X, Sun H and Li L (2011) Evaluation of blends bauxite-calcination-method red mud with other industrial wastes as a cementitious material: properties and hydration characteristics. *Journal of Hazardous Materials* **185(1)**: 329–335, 10.1016/j.jhazmat.2010.09.038.

How can you contribute?

To discuss this paper, please submit up to 500 words to the editor at support@emerald.com. Your contribution will be forwarded to the author(s) for a reply and, if considered appropriate by the editorial board, it will be published as a discussion in a future issue of the journal.